Conference paper

Claudio Mella, Cecilia C. Torres, Cyril Godard, Carmen Claver, Gina Pecchi and Cristian H. Campos*

Heterogeneous palladium SALOPHEN onto porous polymeric microspheres as catalysts for Heck reaction

https://doi.org/10.1515/pac-2018-1225

Abstract: Catalysts based on porous polymeric microspheres were prepared from N,N′-Bis(3,3′-allyl-salicylidene)-o-phenylenediamine Pd(II) (PdAS) metallo-monomer, styrene (STY), and divinylbenzene (DVB) as co-monomers. The effects of the STY/PdAS mass ratio of co-monomers were investigated to synthesize the optimal catalyst. All the prepared materials were characterized by scanning electron microscopy (SEM), N_2 adsorption-desorption isotherms, inductively coupled plasma optical emission spectroscopy (ICP-OES), thermogravimetric analysis (TGA), solid-state diffuse-reflectance UV Vis (DRS UV-Vis) spectrometry, and X-ray photoelectron spectroscopy (XPS). Increasing the PdAS content from 1 to 5 wt%, based on the mass feed of monomers, produced well-defined spherical polymer resins with particle diameters of ~200 μm and high surface areas (>500 m^2/g). XPS spectra shown a unique Pd^{2+} signal associated with the PdAS complex immobilized on a porous resin matrix. The catalytic performances of porous polymer microspheres were evaluated for Heck reaction between iodobenzene and methyl acrylate to produce methyl cinnamate, giving up to 100 % selectivity for the trans-isomer. The resin with 5 wt% PdAS showed the best catalytic activity in methyl cinnamate synthesis. Finally, the best catalytic system was evaluated in octinoxate production producing the target product with the same levels of conversion and selectivity for trans-isomer as was detected for methyl cinnamate synthesis.

Keywords: cross-coupling reactions; Eurasia 2018; immobilization; microsphere resins; palladium catalysis; porous polymers.

Introduction

Metal coordination complexes are extensively used as homogeneous catalysts for many low-scale and industrial processes, especially for the synthesis of important organic building blocks [1, 2]. Particularly,

Article note: A collection of invited papers based on presentations at the 15th Eurasia Conference on Chemical Sciences ($EuAsC_2S$-15) held at Sapienza University of Rome, Italy, 5–8 September 2018.

***Corresponding author: Cristian H. Campos,** Departamento de Físico-Química, Facultad de Ciencias Químicas, Universidad de Concepción, Edmundo Larenas 129, Concepción, Chile, e-mail: ccampos@udec.cl
Claudio Mella: Departamento de Físico-Química, Facultad de Ciencias Químicas, Universidad de Concepción, Edmundo Larenas 129, Concepción, Chile
Cecilia C. Torres: Departamento de Ciencias Químicas, Facultad de Ciencias Exactas, Universidad Andres Bello, Sede Concepción, Autopista Concepción-Talcahuano 7100, Talcahuano, Chile
Cyril Godard and Carmen Claver: Department Physical and Inorganic Chemistry, Universitat Rovira i Virgili, Tarragona, Spain
Gina Pecchi: Departamento de Físico-Química, Facultad de Ciencias Químicas, Universidad de Concepción, Edmundo Larenas 129, Concepción, Chile; and Millenium Nuclei on Catalytic Processes Towards Sustainable Chemistry (CSC), Concepción, Chile

Pd-based homogeneous catalysis has been widely described as the most important methodology for organic C–C coupling reactions [3–7], specifically for the Suzuki, Sonogashira, Stille, Hiyama, and Heck cross-coupling reactions [8, 9]. The main disadvantages of homogeneous catalytic systems are their low recovery capacity and difficulty of their separation from the reaction medium with economic and environmental consequences [10]. Therefore, recent research efforts have been focused on the immobilization of homogeneous catalysts on different insoluble matrixes, to make them both mechanically stable and easily recoverable [11–14].

Different methods for the heterogenization of catalysts involving metal complexes have been reported in cases where covalent immobilization of active homogeneous species has proven an effective pathway for the development of immobilized heterogeneous catalysts [15–17]. There are many different materials available for use as carriers, including silica-based materials, polymeric supports, and inorganic-organic hybrid materials [17–21]. To date, only a few examples of porous polymeric Pd catalysts have been reported. In 2014, Rangel et al. reported the use of polyimine-Pd catalyst for use in Suzuki-Miyaura reactions, affording the corresponding cross-coupling products in excellent yields in water solvent [22]. Sadhasivam et al. also studied imine-Pd-based covalent organic frameworks (COFs) as solid catalysts for C–C coupling reactions; the catalytic system could be recycled more than four times, with only a minor loss of activity [23]. Recently, Xu et al. reported the use hypercrosslinked polymers (HCPs), including N-heterocyclic carbenes (NHCs) and Pd^{2+}, as catalysts with outstanding stability and recyclability for Suzuki–Miyaura cross-coupling reactions of various aryl halides with arylboronic acids [24]. However, despite their success, these Pd-based porous polymers are not considered the most desirable class of catalysts because of their high costs, complex syntheses, air and moisture sensitivity in some cases, inconvenient handling, etc.

In recent decades, Schiff base ligand-mediated Pd-catalyzed C–C cross-coupling reactions have been studied as an economic and environment-friendly alternative to currently active catalytic systems [25–30]. Based on simple, tailor-made syntheses, many structurally different Schiff bases have been prepared, bearing peripheral functional groups on the ligand's structure. This synthetic strategy opens up possibilities of using Schiff bases as building blocks for Pd-based catalysts immobilized onto insoluble supports.

The current efforts in the immobilization of Salen-type palladium (II) complexes are focused in the use of Schiff base ligand, which can suffer polymerization process to provide insoluble resins catalytic materials [25]. Recently, Bi et al. have been reported the synthesis of Salen-ligands into the backbone of HCPs as supports to obtaining heterogenized palladium-complexes for C–C coupling reactions [31]. Based on the above considerations, it is an available strategy to develop efficient heterogeneous catalysts using different Schiff base ligand as building blocks. While this synthetic strategy is undoubtedly advantageous, the metal complex is formed after the ligand immobilization on the surface of the resin. Besides, the chelation processes in polymer-metal systems are far more complicated as compared to low molecular weight analogues, since both reacting agents (polymeric-chelating ligand and metal precursor) can be subjected to very different transformations [32]. Therefore, an alternative route of synthesis starting with a monomer containing a pendant Salen-type palladium (II) complexes (or Pd metallo-monomers) open up the possibility to provide a suitable well-defined supported catalyst with only one specie attached to the surface and easily characterized by spectroscopy techniques.

In this paper, we report a novel synthesis of porous polymeric microsphere catalysts by the suspension polymerization methodology [33–37], employing the metallo-monomer N,N′-bis(3-allyl-salicylidene) o-phenylenediamine Pd(II) (PdAS) Schiff base complex, divinylbenzene (DVB), and styrene (STY) as co-monomers, and 2,2′-azobis(2-methylpropionitrile) (AIBN) as the radical initiator. The main goal was to evaluate the effect of the metallo-monomer loading (1–15 wt%) on the physicochemical properties and catalytic performance of the as-prepared materials. The obtained catalysts were evaluated in a Heck reaction to produce methyl cinnamate (MCIN) as the target molecule from iodobenzene (IB) as the aryl halide and methyl acrylate (MA) as the alkene in the presence of triethylamine (TEA) as the base. Finally, the most active system was evaluated in the production of octinoxate ((RS)-2-Ethylhexyl (2E)-3-(4-methoxyphenyl)prop-2-enoate), which is a fundamental ingredient in sunscreen formulations because of its ability to absorb UV-B rays from the sun [38], thus protecting the skin from damage.

Experimental

Chemicals and reagents

Commercial sodium chloride (NaCl, Merck®), hydroxiethylcellulose (HEC, 99 %, ~90,000 WM, Sigma®), 3-allylsalicylaldehyde (97 %, Sigma®) o-phenylendiamine (99.5 %, Sigma®), palladium (II) acetate ($Pd(CH_3COO)_2$, Merck®), divinylbenzene (DVB, technical grade 80 %, Aldrich®), iodobenzene (IB, 99.0 %, Merck®), 1-iodo-4-methoxybenzene (IBM, 98 % Aldrich), 2-ethylhexyl acrylate (EHA, 98 % Aldrich), octinoxate (2-ethylhexyl trans-4-methoxycinnamate, 98 % Aldrich), methyl cinnamate (MCIN, >99 Aldrich), methanol (MeOH, Merck®), ethanol absolute (EtOH, Merck®), dodecane (Merck®), diethyl ether (Et_2O, Merck®) and acetone (99.5 %, Merck®), Dodecane (≥98.5 Merck), toluene (99.9 % Merck®), were used as received. Triethylamine (TEA 95 % Aldrich®) and styrene (STY, 99 % Aldrich®), Methyl acrylate (MA, 99 % Aldrich®) were purified by distillation process. TEA was distilled at a reduced pressure with CaH_2 and STY and MA were distilled at normal pressure in presence of p-tert-butylcatechol as polymerization inhibitor. 2,2′-azobis(isobutyronitrile) (AIBN, Aldrich®) was purified by recrystallization from methanol and dichloromethane (DCM, 99 % Merck®) was dried with CaH_2 previous to their use.

Synthesis of PdAS

The ligand N,N′-Bis(3,3′-allyl-salicylidene)-o-phenylenediamine (AS) was synthesized as shown in Scheme 1, according to a reported procedure [39]. A 250-mL round-bottomed flask was charged with 3-allylsalicaldehyde (40.0 mmol) in EtOH, and a solution with o-phenylenediamine (20.0 mmol) in 50 mL of EtOH was added to it dropwise. The reaction mixture was then refluxed for 2 h with magnetic stirring. After the reaction, the mixture was cooled at 0 °C for 12 h to obtain a precipitate, which was recrystallized repeatedly from EtOH until the purified ligand AS was obtained as an orange well-defined solid with 81 % yield. ^{1}H NMR (400 MHz, DMSO d_6): δ 13.51 (s, 2H, –OH); 8.94 (s, 2H, –N=C–H); 7.50 (m, 4H, H–Ar); 7.43 (m, 2H, H–Ar); 7.29 (d, 2H, H–Ar); 6.93 (2H, H–Ar); 6.02 (m, 2H, –HC=C–); 5.08 (dd, 2H, HC=C–); 5.0 (dd, 2H, –HC=C–) and 3.49 (d, 4H, Ar–H_2C–C=C); ^{13}C NMR (75 MHz, DMSO d_6): δ 165.90 (Ar–O), 152.49 (Ar–C=N), 143.64, 135.30, 133.60, 132.72, 127.65, 120.01, 115.86, 115.60 and 115.48 (Aromatic carbons), 137.30 (C=CH–), (H_2C=C–), 35.90 (–CH_2–) corresponding to allyl group. Molecular formula $C_{26}H_{24}N_2O_2$; elemental analysis % (nominal in parenthesis): C 79.1(78.8); H 6.5(6.1); N 6.5(7.1). HRMS m/z (M^+ + 1) cal. 397.1898, obs. 397.1904.

Then, the AS ligand (15 mmol) was added to 150 mL of DCM and stirred at room temperature, followed by adding $Pd(CH_3COO)_2$ (15.5 mmol) to the mixture and refluxing for 12 h. A dark-brown precipitate was separated by filtration and washed using MeOH and DCM (4 × 5 mL). The product PdAS was recrystallized from DCM/n-hexane mixture (1:3) with 76 % yield. ^{1}H NMR (400 MHz, DMSO d_6): δ 8.41 (s, 2H, –N=C–H), 7.78 (dq, 2H, H–Ar), 7.30–7.25 (m, 4H, H–Ar), 6.62 (dd, 2H, H–Ar), 6.15 (m, 2H, –HC=C–), 5.28 (dd, 2H, HC=C–), 5.25 (dd, 2H, –HC=C–) and 3.59 ppm (d, 4H, Ar–H_2C–C=C); ^{13}C NMR (75 MHz, DMSO d_6): δ 165.90 (Ar–O), 152.49 (Ar–C=N), 143.64, 135.30, 133.60, 132.72, 127.65, 120.01, 115.86, 115.60 y 115.48 (Aromatic carbons), 137.30 (C=CH–), (H_2C=C–),

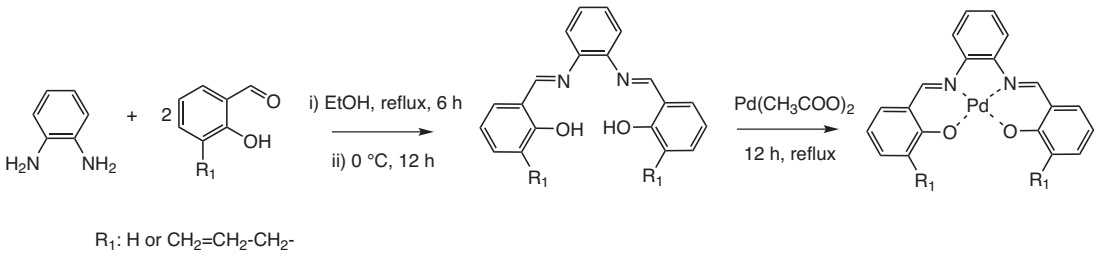

Scheme 1: Ligands synthesis route.

35.90 (–CH_2–) corresponding to allyl group. Molecular formula $C_{26}H_{22}N_2O_2Pd$; elemental analysis % (nominal in parenthesis) C 55.1(62.4); H 3.5 (4.4); N 7.0 (5.6). HRMS m/z (M^+ + 1) calc. 501.0799, obs. 501.0805.

For comparison, the ligand N,N′-bis(salicylidene) o-phenylenediamine (SP) was synthesized in the same way as the AS ligand, producing an orange solid with 78 % yield. ^{1}H NMR (400 MHz, $CDCl_3$): δ 13.04 (s, 2H, –OH); 8.65 (s, 2H, –N=C–H); 7.38 (m, 6H, H–Ar); 7.36–7.24 (m, 4H, H–Ar); 7.06 (d, 2H, H–Ar); 6.93 (t, 2H, H–Ar). ^{13}C NMR (75 MHz, DMSO d_6): δ 164.90 (Ar–OH); 150.60 (Ar–C=N); 142.05, 135.98, 134.71, 126.95, 120.08, 119.60, 116.91 and 114.95 (Aromatic carbons). Molecular formula $C_{20}H_{16}N_2O_2$; elemental analysis % (nominal in parenthesis) C 75.9 (78.8); H 5.1 (6.1); N 8.7 (7.1) HRMS m/z (M^+ + 1) cal. 317.1287, obs. 317.1290.

The homogeneous catalysts Pd(II)-Schiff base complex (PdSP) was synthesized (for comparison) in the same way as PdAS was synthetized, producing a brown solid with 80 % yield. ^{1}H NMR (400 MHz, DMSO d_6): δ 9.19 (s, 2H, –N=C–H); 8.34 (m, 2H, H–Ar); 7.74 (d, 2, H–Ar); 7.45 (m, 4, H–Ar); 7.03 (d, 2H, H–Ar); 6.72 (t, 2H, H–Ar). ^{13}C NMR (75 MHz, DMSO d_6): δ 165.80 (Ar–O), 153.61 (Ar–C=N), 142.85, 136.35, 135.80, 127.90, 120.73, 120.40, 117.15 and 115.51 (Aromatic carbons). Molecular formula $C_{20}H_{14}N_2O_2Pd$; elemental analysis % (nominal in parenthesis) C 58.3 (57.1); H 4.3 (3.4); N 5.3 (6.7). HRMS m/z (M^+ + 1) cal. 421.0174, obs. 421.0176.

Synthesis of high surface PdAS(x)-co-STY polymeric resin

The polymeric resins were synthesized according to reported procedures [33, 34]. In a three-neck polymerization reactor, using 60 wt% of DVB and 1 wt% of AIBN, while the PdAS and STY contents were varied, as shown in Table 1. An inert atmosphere (N_2 gas) was maintained during all the polymerization processes. The co-monomers and initiator were mechanically mixed and the mixture was suspended over an aqueous phase (containing 20 wt% NaCl and 0.2 wt% HMC). The mixture was heated at 70 °C for 14 h, followed by heating to 88 °C for a further 4 h. The monomer/porogen and organic phase (monomer + porogen)/continuous phase were maintained at 1:3 volume ratio. The obtained materials were washed with water for 48 h, followed by washes with DCM and acetone for 24 h each in a Soxhlet apparatus. Finally, the obtained materials were dried at 80 °C in a vacuum oven and were labeled PdAS(x)-STY with x = 0, 1.0, 2.0, 5.0, 10 and 15 wt% (nominal loading of PdAS), where x = 0 is the control material.

Characterization techniques

NMR spectra were recorded in a Bruker Ascend TM 400 MHz spectrometer operating at 400 (^{1}H) and 75 (^{13}C) MHz and chemical shifts reported as δ values (ppm) with the residual solvent signal as the internal reference. ESI-Q TOF MS spectra were obtained in positive mode on a QTOF Micro mass spectrometer (Waters, Manchester, UK) in smart tube mode with capillary voltage set at 3.5 kV, cone voltage at 30 V, source temperature at 100 °C and temperature of desolvation at 120 °C. The samples were introduced by infusion in an acetonitrile solution. Chemical organic analyses were performed on a Fisons – EA-1108 CHNS-O Element

Table 1: Nominal composition of PdAS(x)-STY of polymeric resins.

Label	wt%			
	DVB	STY	PdAS	AIBN
PdAS(0)-STY	60	39	0	1
PdAS(1)-STY	60	38	1	1
PdAS(2)-STY	60	37	2	1
PdAS(5)-STY	60	34	5	1
PdAS(10)-STY	60	29	10	1
PdAS(15)-STY	60	24	15	1

Analyzer. Chemical inorganic analysis of the samples was conducted by inductively coupled plasma optical emission spectrometry (ICP-OES) using a Spectro Arcos instrument. Samples were digested in a mixture of concentrate HNO_3 and H_2SO_4 under microwave treatment on a Milestone Srl equipment model Ethos Easy and then diluted for the analysis. Differential thermal analysis and thermogravimetry (DTA/TG) experiments were performed at a heating rate of 10 °C min^{-1} up to 1000 °C with N_2 flow of 8.0 mL/min in NETZSCH TG equipment model 209F1 Iris using a weight of 3.0 mg of sample. The nitrogen adsorption isotherms obtained on a Micromeritics apparatus Model TriStar II Series 2 at –196 °C and the specific area calculated using the B.E.T method and the pore size distribution and pore volume were calculated by BJH method. The catalysts morphology was characterized by Scanning Electron Microscopy (SEM) on TESCAN equipment, Vega 3 LMU model, coupled to EDS probe. Solid state UV-VIS spectroscopy analysis was recorded on a Thermo Scientific Bio UV-Vis Spectrophotometer equipment model Evolution 260 and liquid UV-vis spectra was recorded on a spectroquant equipment model Pharo 300, using CH_2Cl_2 as solvent. X-ray photoelectron spectroscopy (XPS, RQ-300 X-ray Source, STAIB Instruments) was performed to determine the binding energies of the samples using Al radiation (hν = 11486.6 eV) operated at 75 W.

Catalytic activity

To evaluate the catalytic performances of the heterogeneous Pd-coordinated catalysts the IB:Pd and IB:MA:TEA molar ratios were 2000:1 and 1:1.25:2, respectively. The reaction was carried out in a Parr-type semi-batch reactor with a reactant pre-chamber. The reactions were studied at 120 °C in Ar (5.5 bar), using DMF as solvent (50 mL) at 770 rpm of magnetic stirring. All experiments were carried out in the absence of any external mass transfer limitations (not included). The heating was carried out for the solution of IB and dodecane in DMF until the desired temperature was reached. After thermal equilibrium, MA and TEA were added from the pre-chamber. The rate progress was measured in terms of IB consumption by GC analysis, using dodecane as the internal standard (908 μL dodecane, 0.8 mmol). Non-invasive aliquots (~50 μL) were taken from the reaction mixture at different times and added to 1 mL water, followed by extraction with Et_2O (1000 μL) and washing with 1 mL of brine. The organic layer was analyzed by a Perkin Elmer GC model Clarus 680, equipped with a Elite-MS5 capillary column, and the retention times were compared with the corresponding GC commercial standards. For evaluating the activity in the production of Octinoxate, 1-iodo-4-methoxybenzene (IBM) was used as the aryl halide and 2-ethylhexyl acrylate (EHA) as the activated alkene under the same reaction conditions optimized for MCIN production. Reusability tests was also performed for the most active and selective catalyst. For the reusability test, following the initial catalytic run, the catalyst was collected by direct filtration from the reactor, and the recovered catalyst was subjected to three subsequent catalytic cycle under identical conditions.

Results and discussion

Synthesis and characterization of PdAS metallo-monomer

According the characterization techniques, the proposed symmetrical Pd(II) complexes, PdSP and PdAS were successfully synthesized. The evidence of the Pd-based complexes formation can be followed by the disappearance of the –OH signal at 13.51 ppm for AS and 13.04 ppm for SP in the ^1H NMR spectra and the structure of the ligands ascertained by the ESI-Q TOF MS characterization.

In our initial screening experiments, the co-polymerization of AS ligand and PdAS metallo-monomer to prepare the microsphere polymeric resins were investigated (Supplementary material). The AS ligand co-polymerization (5 wt%) with STY was conducted under the same reaction conditions employed for the catalysts described in the experimental section. To obtain metal complexes on the material surface, resin was contacted

with $Pd(CH_3COO)_2$ for 12 h by reflux in DCM. XPS characterization of the as-prepared catalyst revealed the presence of both Pd^{2+} and Pd^0 species. We also confirmed the presence of Pd metallic nanoparticles by X-ray diffraction (XRD) and transmission electron microscopy (TEM) characterization. Although metallic Pd nanoparticles have been used as the active phase in Heck reactions [40–42], our aim in this study was the evaluation of homogeneous PdAS catalysts immobilized onto porous microsphere resins and their effect on the catalytic performance. The PdAS metallo-monomer ensured the inclusion of the Heck reaction catalysts on the backbone chain of the resins to avoid the formation of a metal complex by post-polymerization immobilization.

Polymeric resins characterization

The SEM micrographs for all the synthesized PdAS(x)-STY materials are shown in Fig. 1. The control PdAS(0)-STY resin formed well-defined spherical granules with a mean particle size of 190 μm. The incorporation of the PdAS *co*-monomer in the materials resulted in spherical beads of similar sizes than the PdAS(0)-STY control material for the catalysts PdAS(x)-STY with x = 1, 2, and 5. For PdAS(x)-STY catalysts with x = 10 and 15, amorphous and irregular microparticles were formed.

The N_2 adsorption-desorption isotherms of the PdAS(x)-STY catalysts (Fig. 2) confirm the porous properties of these resins. All the materials exhibited type IV isotherms, associated with particle aggregates, which is typical for mesoporous materials. The hysteresis loop showed variation in pore morphology at higher PdAS amounts, from a typical H1 type for PdAS(x)-STY with x = 0, 1, 2, and 5, to a H2-type associated with a laminar material for x = 10 and 15. The apparent surface areas were estimated from the Brunauer–Emmett–Teller (BET) equation (Table 2) and these results are shown in Fig. 2 (inset). The variation of the BET surface area (S_{BET}) as a function of PdAS content showed a volcano-type curve, in which x > 5 wt% was accompanied by a drastic reduction in surface area, reaching almost 100 m^2/g for PdAS(15)-STY catalyst.

The amount of Pd in PdAS(x)-STY catalyst was measured by ICP-OES (Fig. 3); the real values were found to be lower than the nominal ones used in the preparation of the porous polymer resins. A saturation value was obtained at nominal 15 wt% PdAS because the catalysts has the same Pd loading as the material at nominal 10 wt% PdAS.

A well-defined microsphere morphology, large S_{BET} (~600 m^2/g), and a continuous incorporation of the PdAS complex with increasing metallo-monomer nominal loading from the non-modified PdAS(0)-STY to the PdAS(x)-STY x: 1, 2, 5 can be seen. Conversely, PdAS(10)-STY and PdAS(15)-STY display irregular shapes, significantly reduced S_{BET}, and the same Pd content in the synthesized materials.

This trend can be explained by the experimental conditions employed in the suspension polymerization of the *co*-monomers PdAS, STY, and DVB. The morphologies of the beads are shown to be affected by the solubility parameters of the monomers and porogens [43–45]. Recently, Cai et al. have reported an interesting study on the preparation of cross-linked poly-(acrylonitrile-co-STY-co-DVB) terpolymer beads with different monomer contents, employing suspension polymerization in the presence of a co-porous agent (toluene, cyclohexane, and/or heptane) [46]. They observed a change in the nature of the microspheres (break to produce amorphous agglomerates) with increasing acrylonitrile *co*-monomer content in the resin compositions. This result is in line with the trend observed in our PdAS(x)-STY materials, because different STY/PdAS mass ratios were employed. The physicochemical natures of both *co*-monomers are distinctly different, PdAS being a polar molecule and STY being a low-polarity molecule. This property could affect the solubility parameters of the *co*-monomer mixture and the toluene porogen during the polymerization process in a similar manner to that reported by Cai et al.

Another import parameter to consider in the preparation of these materials is the reactivity ratio of the *co*-monomers in the polymerization medium. A series of mathematical models has been reported to predict reactivity ratios of monomers participating in free radical *co*-polymerizations [47, 48]. Among them, the Alfrey-Price Q-e scheme is the most widely used. The PdAS and DVB structures possess two propagation centers, while STY has only one vinyl functionality. To simplify the approximation, we considered the Q-e predictor $CH_2{=}CH_2{-}C_6H_5$ for both STY and DVB, and $CH_2{=}CH_2{-}CH_2{-}CH_3$ for PdAS. The relation of the reactivity ratios for the co-monomers is:

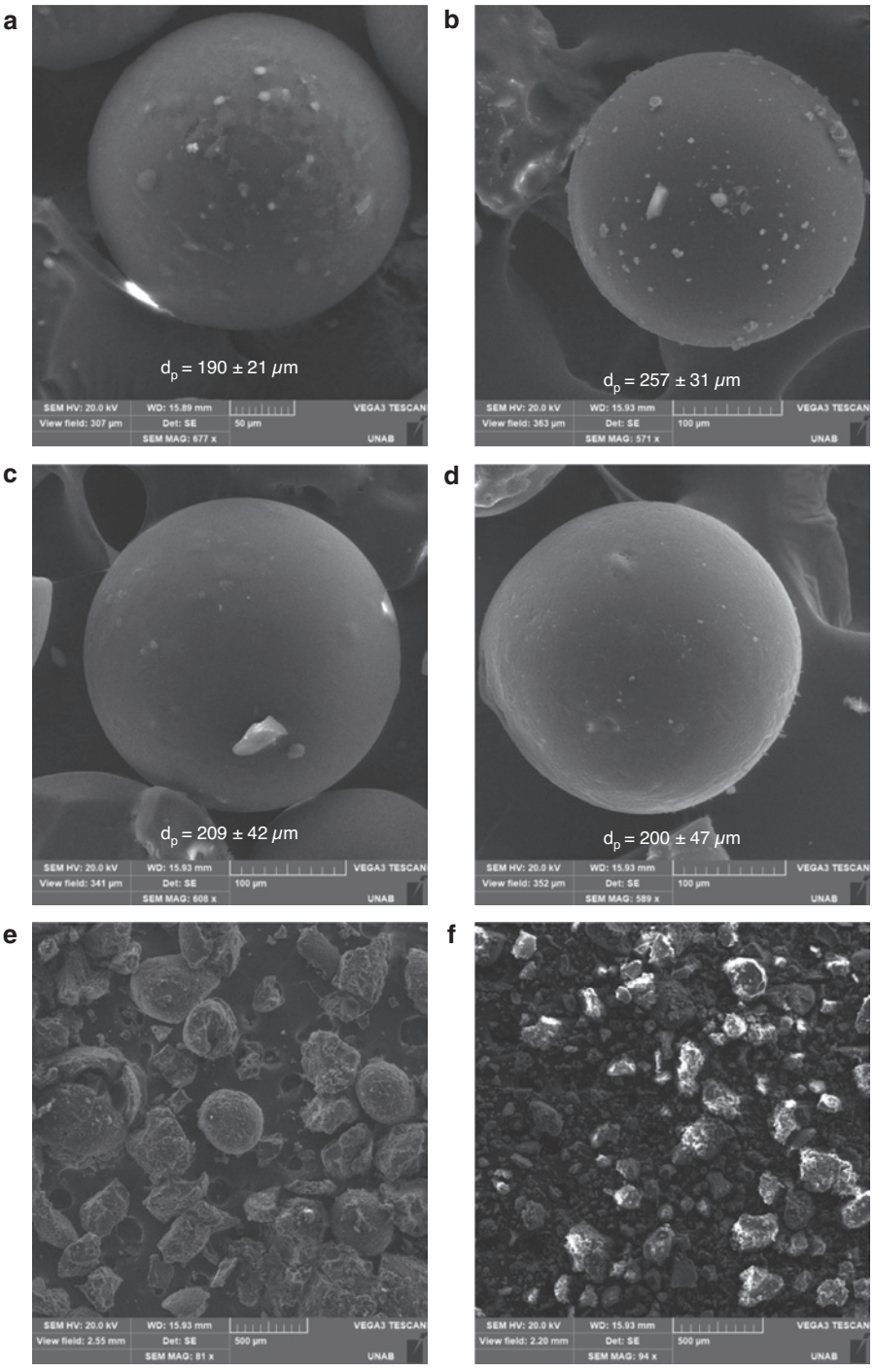

Fig. 1: SEM micrographs for the synthetized resins. (a) PdAS(0)-STY. (b) PdAS(1)-STY. (c) PdAS(2)-STY. (d) PdAS(5)-STY. (e) PdAS(10)-STY and (f) PdAS(15)-STY.

$$r_1 r_2 = e^{[-(e_1 - e_2)^2]} \tag{1}$$

where e_1 and e_2 are proportional to the residual charges in the respective reacting groups corresponding to the tabulated data. The reactivity values for of STY ($e = -0.80$) [49] and the estimated PdAS ($e = -0.06$) [49] are $r_{STY} r_{STY} = 1.0$ and $r_{STY} r_{PdAS} = 0.58$, respectively. According with this approximation, STY and DVB are more reactive than PdAS toward the formation of co-polymers. At lower PdAS loadings, the effect is considerable, providing

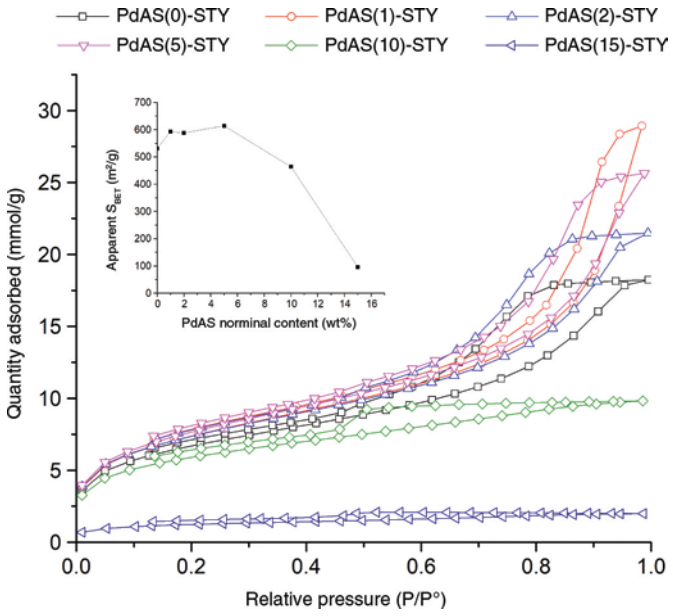

Fig. 2: N_2 adsorption-desorption isotherm (inset presents apparent S_{BET} in function of PdAS nominal content on the solids structure).

Table 2: Heck Reaction for PdAS(x)-STY with x = 0, 1, 2 and 5 catalysts at 60 min of reaction.

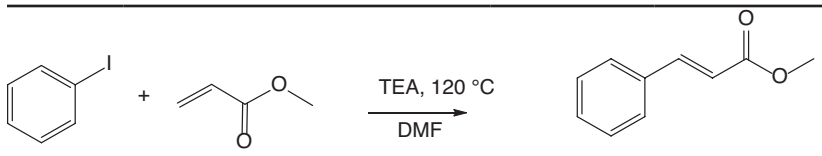

Catalyst	IB conversion (%)	cis:trans isomers
–	0.1	0:100
	0.3[a]	
PdSP	70.4	0:100
	99.2[b]	
PdAS(0)-STY	0.5	0:100
	0.6[a]	
PdAS(1)-STY	15.4	0:100
	99.8[b]	
PdAS(2)-STY	62.2	0:100
	99.2[b]	
PdAS(5)-STY	72.4	0:100
	99.2[b]	

[a]Conversion measured at 720 min (12 h) of reaction, [b]conversion measured at 240 min of reaction.

PdAS(x)-STY resins (x = 1, 2, and 5) with spherical shape and higher surface area. Conversely, increasing of PdAS content at nominal loadings higher than 5 wt% provides the difficult-to-prepare DVB-PdAS-STY *co*-polymers with homogeneous insertion of PdAS in the resin structure. This behavior is supported by the ICP-OES characterization, where PdAS(10)-STY and PdAS(15)-STY showed similar Pd loadings despite having been prepared at higher nominal Pd contents.

According to the solubility parameters and reactivity ratio of the co-monomers, the morphology and physicochemical characteristics of PdAS(10)-STY and PdAS(15)-STY could be explained by the accumulation of PdAS in the polymerization medium, which collapsed the beads, providing amorphous and non-porous materials.

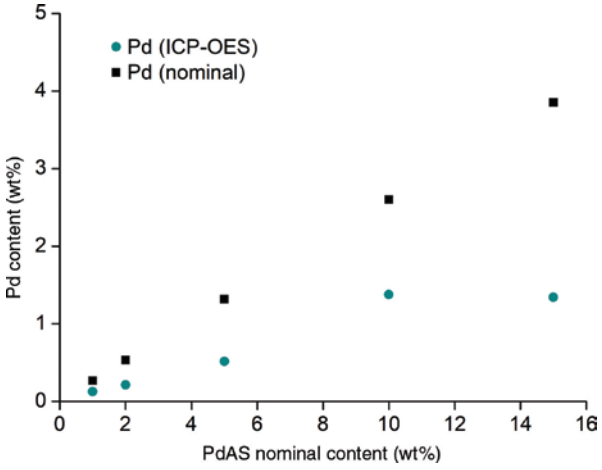

Fig. 3: Nominal and real Pd content in PdAS(x)-STY catalysts.

Figure 4 shows the TGA-DTGA curves for all the as-prepared catalysts. As shown, the materials obtained from all the resins were stable in N_2 below 390 °C and exhibited one decomposition region corresponding to the decomposition of the crosslinked divinylbenzene-styrene (DVB-STY) structures. It was also observed that the mass loss depended on the PdAS content. The decomposition temperatures for 50 % weight loss (T_{50}) for the materials obtained at different PdAS contents are shown in Fig. 4. The shift T_{50} of the PdAS(x)-STY ($x \neq 0$) resins to slightly higher temperatures indicate the improved thermal stability compared with the PdAS(0)-STY control material.

XPS was employed as a qualitative method to analyze the chemical state of the immobilized Pd complex, comparing PdAS(x)-STY catalysts with the coordination compound PdAS. Both core levels and auger emission were clearly identifiable for PdAS as shown in Fig. 5. The Pd $3d_{5/2}$ spectra showed peaks at the binding energy (BE) of 338.6 eV, with a spin-orbital splitting at 5.27 eV, while the C 1s and N 1s spectra present peaks at BEs of 285 and 400.0, respectively. Furthermore, the Pd $3d_{5/2}$ and N 1s core levels on all the catalysts present identical BEs compared with the free complex, confirming the immobilization of the PdAS coordination compound. On the other hand, PdAS(x)-STY ($x = 1$, 2, and 5) catalysts present weak contributions of Pd and N species due to lower PdAS loading onto the resins.

We proposed that the main distribution of this *co*-monomer is located inside the porous matrix. It is easy to appreciate an increase in Pd $3d_{5/2}$ signals, as shown in the inset of Fig. 5 which is in agreement with ICP-OES characterization. The PdAS(10)-STY and PdAS(15)-STY catalysts showed the highest Pd loading (~1.35 wt%), but a different profile in the definition of signals was detected. Although both catalysts possess almost the same Pd loading, the lowest apparent S_{BET} of PdAS(15)-STY could explain the increase in Pd BE intensity by the exposition of the metallo-monomer on the resin surface.

Solid-state DRS UV-vis spectra were obtained for all the PdAS(x)-STY materials (Fig. 6a). Liquid-phase UV-vis spectra for PdAS (Fig. 6b) showed the following transition bands: $\pi \rightarrow \pi^*$ at 241 nm, $n \rightarrow \pi^*$ between 336 and 355 nm, and a typical charger transfer (C-T) and d–d transition band for Schiff base-metal complexes at 481 nm [50]. As expected, the PdAS(0)-STY material mainly absorbed in the UV range (aromatic moieties absorption), whereas PdAS(x)-STY ($x \neq 0$) catalysts possessed broader absorption range up to 300 nm, with absorption maxima between 400 and 500 nm, attributed to the presence of PdAS on the resin structure.

Catalytic activity

Heck coupling between IB with MA was selected to evaluate the catalytic activity of the PdSP homogeneous catalyst and PdAS(x)-STY ($x = 1$, 2, and 5) catalysts. According to the characterization results, the PdAS(10)-STY and PdAS(15)-STY catalysts were not considered because they did not show the microsphere shape.

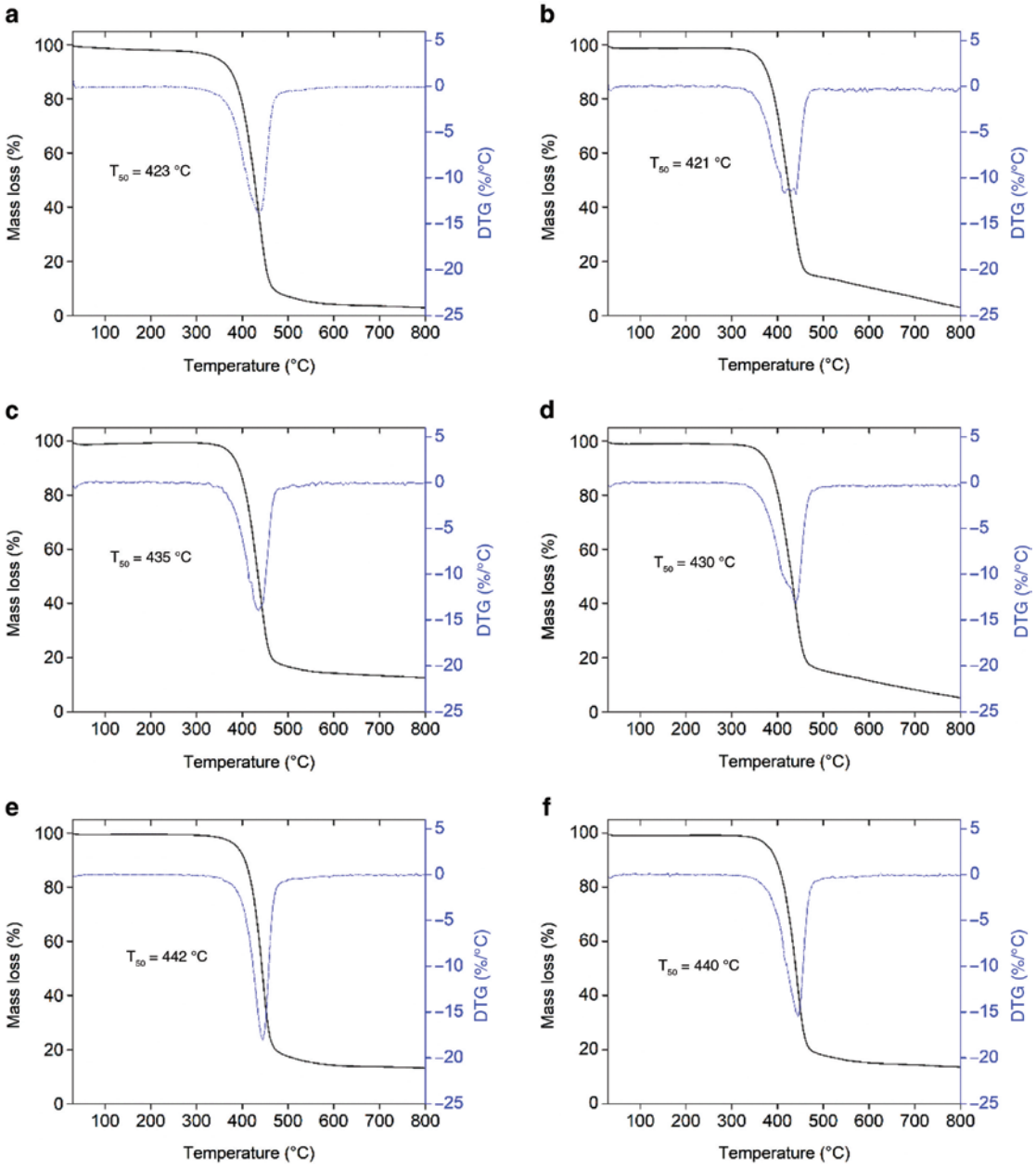

Fig. 4: Thermogravimetric profiles of PdAS(x)-STY materials. (a) PdAS(0)-STY, (b) PdAS(1)-STY, (c) PdAS(2)-STY. (d) PdAS(5)-STY. (e) PdAS(10)-STY and (f) PdAS(15)-STY.

As a control experiment, the reactions with PdAS(0)-STY and without catalyst were studied under the reaction conditions described in the experimental section. Negligible activity was observed after 12 h of reaction as shown in Table 2. All the evaluated catalysts were active in the production of MCIN, yielding the trans-isomer as the only product. No geminal C–C coupling product was detected.

On the other hand, the catalysts presented an increasing trend in activity: PdAS(1)-STY < PdAS(2)-STY < PdAS(5)-STY ≈ PdSP. This behavior could be attributed to the nature of the PdAS(x)-STY catalyst. Although all the catalysts showed similar physicochemical properties (mean microsphere diameter and S_{BET}) and the catalytic activity was evaluated at Pd:IB = 2000 (using the Pd values measured by ICP-OES), the surface distribution of the PdAS immobilized catalysts was more homogeneous in the PdAS(5)-STY catalysts.

Finally, the PdAS(5)-STY catalyst was evaluated in the production of octinoxate by the C–C coupling of IBM and EHA as shown in Fig. 7. The IBM consumption, and thus the conversion, was maximum after 120 min

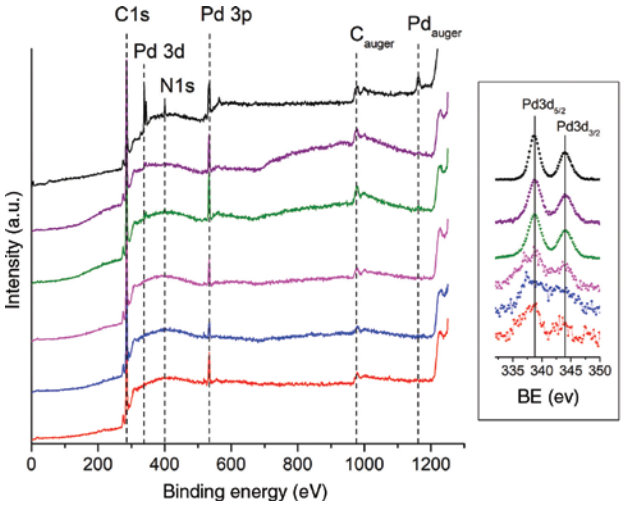

Fig. 5: XPS spectrum (Pd3d region; inset) of the PdAS complex and PdAs(x)-STY catalysts. PdAS complex (black), PdAS(1)-STY (red), PdAS(2)-STY(blue), PdAS(5)-STY (magenta), PdAS(10)-STY (green) and PdAS(15)-STY (purple).

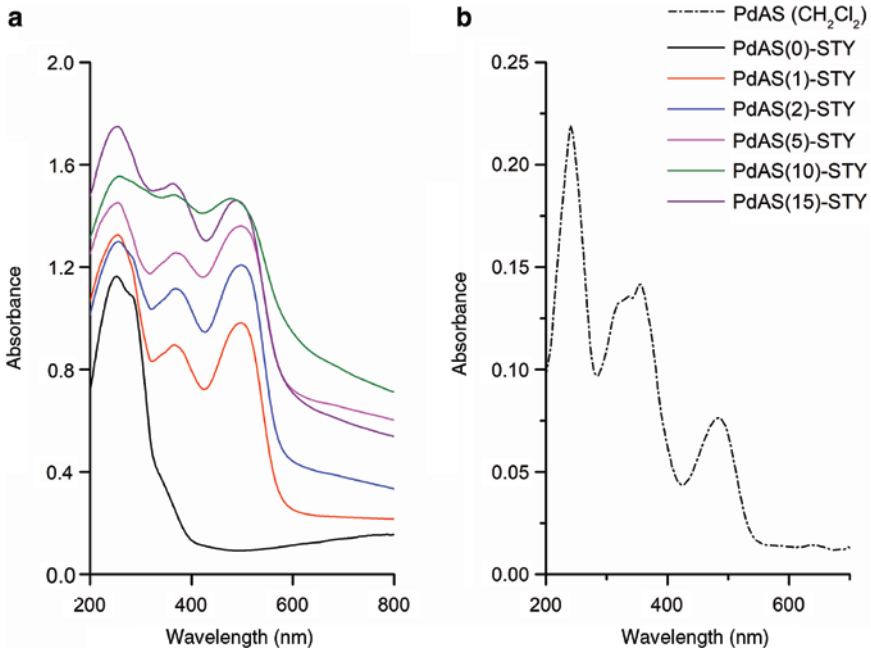

Fig. 6: UV-Vis characterization for PdAS and PdAS(x)-STY materials. (a) DRS UV-Vis profile of PdAS(x)-STY catalysts and (b) UV-Vis spectra for PdAS on CH_2Cl_2 as solvent.

of reaction, producing octinoxate as the only product. For comparison, the catalytic activity of PdAS(5)-STY in the production MCIN is included. In both reactions, the catalytic performance showed similar profiles, reaching maximum conversion after 120 min and the trans-isomer as the only reaction product for both MCIN and octinoxate synthesis.

Concerning the critical feature of reusability, for the PdAS(5)-STY catalyst, consecutive catalytic cycles were carried out. On the basis of our studies, PdAS(5)-STY catalyst was used for three cycles with only minor loss of yields reaching the maximum of conversion level at high reaction time in the second and third catalytic cycle as shown in Fig. 8.

To detect Pd leaching, it was also measured by AAS the Pd content in the post-reaction medium. The absence of Pd leaching up to the second run indicates the high stability of the synthesized started PdAS

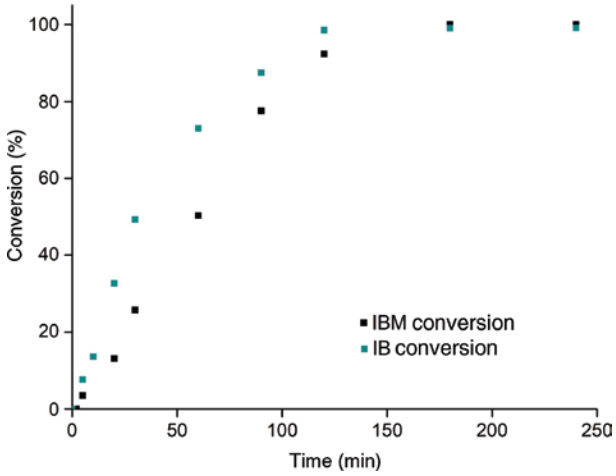

Fig. 7: Conversion level for PdAS(5)-STY in function of aryl halide consumption in the production of octinoxate (black label) and MCIN (green label) for PdAS(5)-STY catalyst.

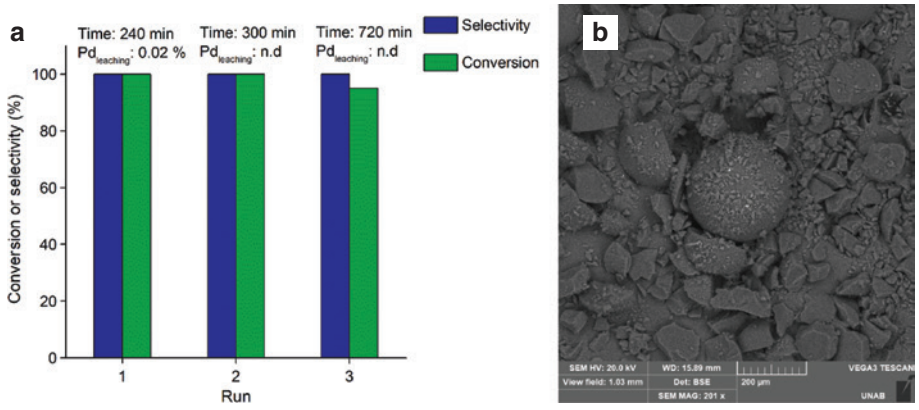

Fig. 8: Recycle study for PdAS(5)-STY catalyst in Heck reaction of IB and MA. (a) Catalytic activity and leaching measurements and (b) SEM characterization after third cycle.

metal-monomer, and the changes in the SEM micrograph of the third catalytic run catalyst shown in (Fig. 8b) indicates the dependence on their textural properties. It is proposed that the loss of activity in the PdAS(5)-STY catalyst is attributed to a gradual collapsed process with appearance of agglomerated and irregular broken microparticles.

Conclusion

A novel porous polymer microsphere resin, including a Pd-based metallo-monomer, with catalytic activity in Heck reaction, was prepared using suspension polymerization. XPS and DRS UV-Vis characterizations confirm the presence of the Pd metallo-monomer on the resin matrix as Pd^{2+}-complexes after the polymerization process. SEM, N_2 adsorption-desorption isotherms, and ICP-OES characterization showed that the materials possess limited tolerance for the incorporation of Pd metallo-monomer. At Pd metallo-monomer contents ranging from 1 to 5 wt%, based on the monomer mass feed, the resins showed well-defined microsphere shape and apparent surface areas of ~600 m^2/g. An increase in the Pd metallo-monomer content (>10 wt%) collapses the suspension, producing irregular shapes and materials with lower apparent surface areas. These new solid-based microsphere resins are active and selective in C–C coupling of aryl halides with

alkenes, showing that the optimal Pd metallo-monomer loading was 5 wt%. These catalysts displayed high activity and selectivity in the synthesis of both methyl cinnamate and octinoxate, only producing the respective trans-isomers.

Acknowledgements: The authors thank CONICYT FONDECYT 1170083, FONDECYT 11170095, FONDECYT 11160468 and Unidad de Equipamiento Científico – MAINI, Universidad Católica del Norte, for the XPS analysis (Conicyt-Programa FONDEQUIP XPS EQM 140044 2014-2016). C. Mella thanks to CONICYT Grant 21150195 for his PhD fellowship. C.C. Torres thanks to CONICYT, PAI/Concurso Nacional inserción de Capital Humano Avanzado en la Academia Convocatoria año 2017 PAI79170027. The authors thank to Dr. Joel B. Alderete of the Instituto de Química de Recursos Naturales – Universidad de Talca, Chile for his collaboration with the ESI-MS/MS analysis.

References

[1] H.-U. Blaser, A. Indolese, A. Schnyder. *Curr. Sci.* **78**, 1336 (2000).
[2] J. Magano, J. R. Dunetz. *Chem. Rev.* **111**, 2177 (2011).
[3] E.-i. Negishi. *J. Organometal. Chem.* **653**, 34 (2002).
[4] Á. Molnár. *Chem. Rev.* **111**, 2251 (2011).
[5] C. C. C. Johansson Seechurn, M. O. Kitching, T. J. Colacot, V. Snieckus. *Angew. Chem., Int. Ed.* **51**, 5062 (2012).
[6] C. Bolm. *J. Org. Chem.* **77**, 5221 (2012).
[7] C. C. C. Johansson Seechurn, A. DeAngelis, T. J. Colacot. "Introduction to new trends in cross-coupling", in *New Trends in Cross-Coupling: Theory and Applications*, T. Colacot (Ed.), Chapter 1, pp. 1, The Royal Society of Chemistry, USA (2015).
[8] A. Jutand. "Mechanisms of the Mizoroki–Heck reaction", in *The Mizoroki–Heck Reaction*, M. Oestreich (Ed.), Chapter 1, pp. 1, John Wiley & Sons, Ltd., Chichester, UK (2009).
[9] I. P. Beletskaya, A. V. Cheprakov. *Chem. Rev.* **100**, 3009 (2000).
[10] P. T. Anastas, M. M. Kirchhoff, T. C. Williamson. *Appl. Catal. A.* **221**, 3 (2001).
[11] I. R. Shaikh. *J. Catal.* **2014**, 35 (2014).
[12] M. J. Hinner, M. Grosche, E. Herdtweck, W. R. Thiel. *Z. Anorg. Allg. Chem.* **629**, 2251 (2003).
[13] D. Grekov, T. Vancompernolle, M. Taoufik, L. Delevoye, R. M. Gauvin. *Chem. Soc. Rev.* **47**, 2572 (2018).
[14] S. Fukuzumi, Y.-M. Lee, W. Nam. *ChemCatChem* **10**, 1686 (2018).
[15] I. F. J. Vankelecom, P. A. Jacobs. "Catalyst immobilization on inorganic supports", in *Chiral Catalyst Immobilization and Recycling*, D. E. De Vos, I. F. J. Vankelecom, P. A. Jacobs (Eds.), Chapter 2, pp. 19, Wiley-VCH Verlag GmbH, Weinheim, Germany (2007).
[16] F. Cozzi. "Catalyst immobilization strategy: some general considerations and a comparison of the main features of different supports", in *Recoverable and Recyclable Catalysts*, M. Benaglia (Ed.), Chapter 15, pp. 427, Wiley-VCH Verlag GmbH, Weinheim, Germany (2009).
[17] X. S. Zhao, X. Y. Bao, W. Guo, F. Y. Lee. *Mater. Today* **9**, 32 (2006).
[18] A. Zamboulis, N. Moitra, J. J. E. Moreau, X. Cattoen, M. Wong Chi Man. *J. Matter. Chem.* **20**, 9322 (2010).
[19] A. Corma, H. García, F. X. Llabrés i Xamena. *Chem. Rev.* **110**, 4606 (2010).
[20] V. Polshettiwar, Á. Molnár. *Tetrahedron* **63**, 6949 (2007).
[21] A. C. Albéniz, N. Carrera. *Eur. J. Inorg. Chem.* **2011**, 2347 (2011).
[22] E. Rangel Rangel, E. M. Maya, F. Sánchez, J. G. de la Campa, M. Iglesias. *Green Chem.* **17**, 466 (2015).
[23] V. Sadhasivam, R. Balasaravanan, C. Chithiraikumar, A. Siva. *ChemistrySelect* **2**, 1063 (2017).
[24] S. Xu, K. Song, T. Li, B. Tan. *J. Matter. Chem. A* **3**, 1272 (2015).
[25] P. Das, W. Linert. *Coord. Chem. Rev.* **311**, 1 (2016).
[26] M. Keleş, H. Keleş, D. M. Emir. *Appl. Organomet. Chem.* **29**, 543 (2015).
[27] A. Gogoi, A. Dewan, G. Borah, U. Bora. *New J. Chem.* **39**, 3341 (2015).
[28] N. Shahnaz, B. Banik, P. Das. *Tetrahedron Lett.* **54**, 2886 (2013).
[29] W. N. W. Ibrahim, M. Shamsuddin. *Cryst. Struc. Theory Appl.* **1**, 5 (2012).
[30] P. G. Cozzi. *Chem. Soc. Rev.* **33**, 410 (2004).
[31] J. Bi, Y. Dong, D. Meng, D. Zhu, T. Li. *Polymer* **164**, 183 (2019).
[32] N. T. S. Phan, M. Van Der Sluys, C. W. Jones. *Adv. Synth. Catal.* **348**, 609 (2006).
[33] C. H. Campos, J. B. Belmar, S. E. Jeria, B. F. Urbano, C. C. Torres, J. B. Alderete. *RSC Adv.* **7**, 3398 (2017).
[34] J. Wei, X. Zhao, J. Yan. *J. Appl. Polym. Sci.* **92**, 2681 (2004).
[35] J. Wei, X. Y. Bai, J. Yan. *Macromolecules* **36**, 4960 (2003).

[36] D.-x. Hao, F.-l. Gong, W. Wei, G.-h. Hu, G.-h. Ma, Z.-g. Su. *J. Colloid Interface Sci.* **323**, 52 (2008).
[37] Y. Jun, X. Rongnan, Y. Juntan. *J. Appl. Polym. Sci.* **38**, 45 (1989).
[38] A. R. Nunes, Í. G. P. Vieira, D. B. Queiroz, A. L. A. B. Leal, S. Maia Morais, D. F. Muniz, J. T. Calixto-Junior, H. D. M. Coutinho. *Adv. Pharmacol. Sci.* **2018**, 9 (2018).
[39] F. F. He, H. Q. Wang, Y. Y. Wang, X. F Wang, H. S. Zhang, H. L. Li, J. H. Tang. *J. Radioanal. Nucl. Chem.* **295**, 167 (2013).
[40] R. P. Jumde, M. Marelli, N. Scotti, A. Mandoli, R. Psaro, C. Evangelisti. *J. Mol. Cat. A: Chem.* **414**, 55 (2016).
[41] A. Balanta, C. Godard, C. Claver. *Chem. Soc. Rev.* **40**, 4973 (2011).
[42] J. Zhu, J. Zhou, T. Zhao, X. Zhou, D. Chen, W. Yuan. *Appl. Catal., A.* **352**, 243 (2009).
[43] M. T. Gokmen, F. E. Du Prez. *Prog. Polym. Sci.* **37**, 365 (2012).
[44] B. Brooks. *Chem. Eng. Technol.* **33**, 1737 (2010).
[45] S. Shi, T. P. Russell. *Adv Mater* **30**, 1800714 (2018).
[46] Y. Cai, W. Yan, X. Peng, M. Liang, L. Yu, H. Zou. *J. Appl. Polym. Sci.* **136**, 46979 (2019).
[47] S. C. Rogers, W. C. Mackrodt, T. P. Davis. *Polymer* **35**, 1258 (1994).
[48] D. Zaremba, H. Menzel, W. Kowalsky, H.-H. Johannes. *Mater. Chem. Phys.* **209**, 227 (2018).
[49] R. Z. Greenley. *J. Macromol. Sci. Part A Pure Appl. Chem.* **14**, 427 (1980).
[50] A. Choudhary, S. Kumari, S. Ray. *ACS Omega* **2**, 6636 (2017).

Supplementary Material: The online version of this article offers supplementary material (https://doi.org/10.1515/pac-2018-1225).